A 3D Numerical Study of Arcjet Thrusters: Effect of Electrode Configuration on Performance of Arcjet thruster

IEPC-2019-744

Presented at the 36th International Electric Propulsion Conference
University of Vienna • Vienna, Austria
September 15-20, 2019

Hari prasad N[1], Deepak Akhare[2], Amit Kumar[3],Jayachandran T[4],
Department of Aerospace Engg, Indian Institute of Technology Madras, Chennai, India, 600036

Abstract: A 3D numerical model have been developed to study the unsymmetrical behavior of hydrogen plasma flow, inside a lower power arcjet thruster. A complete set of governing equations includes those of conservation of mass, momentum, and energy for a viscous, compressible flow with the electromagnetic body forces and Joule (Ohmic) heating as source terms in momentum and energy equations respectively are solved. In the present work, a 3D numerical CFD code for hydrogen arcjet (NASA 1kW) was developed and validated against existing experimental data to assess the effect of cathode configuration (cathode tip offset from the thruster axis) on thruster performance.

Nomenclature

$\boldsymbol{B}$	=	magnetic induction vector
D_i	=	diffusion of pure species
$D_{i,j}$	=	binary diffusion of i, j species
D_{amb}	=	ambipolar diffusion
$\mathbf{E}$	=	electric field vector
F	=	thrust
I	=	electric current
I_{sp}	=	specific impulse
$\boldsymbol{J}$	=	current density vector
L_h, L_e	=	energy loss rate of heavy and electron species
M_i	=	molecular weight of species
T	=	gas temperature
$\boldsymbol{V}$	=	velocity vector
P	=	pressure
Q_{ij}	=	collision cross section for i, j species encounter
$\hat{R}$	=	universal gas constant
Z_i	=	partition function of species
$\overline{c}$	=	mean velocity
ds	=	elemental area
$d\Omega$	=	elemental volume
e_t	=	total energy
h	=	Plank's constant
h_t, h_i,	=	total and species enthalpy

[1] PhD scholar, Department of Aerospace Engg., hari25.astro@gmail.com
[2] MS scholar, Department Aerospace Engg., akharedeepak@gmail.com
[3] Professor, Department Aerospace Engg., amitk@ae.iitm.ac.in.
[4] Visiting professor, Department Aerospace Engg., t_jayachandran@ae.iitm.ac.in.

κ_t, κ_i = total and species thermal conductivity
k_b = Boltzmann constant
k_f, k_b = forward and backward reaction rate coefficient
$\dot{m}$ = mass flow rate
m_i = mass of species
$\boldsymbol{n}$ = normal vector
n_i = number density of species
$\dot{n}_i$ = production rate of species
n_n = number density of neutral atoms
$\boldsymbol{q}$ = heat flux vector
u, v, w = velocity components in x, y, z directions
y_i = mass fraction of species
ρ = density
$\bar{\bar{\boldsymbol{\tau}}}$ = viscous stresses
Σ = electrical conductivity
α = degree of ionization
σ = electrical conductivity
ϕ = electric potential
μ_t, μ_i = total and species coefficient of viscosity
μ_0 = magnetic permeability of free space
ϵ_0 = permittivity of free space
ε_i = ionization energy
ε_d = disassociation energy
$\overline{\Omega}_{i,j}^{(l,s)}$ = average collision integral between i, j species

I. Introduction

ELECTRIC Arcjet thrusters are the replacement for conventional chemical thrusters used for North-South station keeping and satellite maneuvering. To increase the life of the satellites, there is a move towards using electric propulsion-based thrusters owing to the higher specific impulse. In arcjet thrusters, gaseous fuel is heated electro-thermally by utilizing high-temperature DC arc, passing through the constrictor. In space missions, arcjet thruster needs to operate for several hundred hours during which cathode experiences high electrical and thermal stresses. This stresses in turns lead to the severe erosion of the electrode, insulators, and seal joints. Of these components erosion of cathode affects the performance of the arcjet thruster more severely[1]. Arcjet cathode erosion has been the subject of interest over the past few decades to enhance the performance and life of the arcjet thruster[2,3].High electrical and thermal stresses on the electrode may lead to change in shape and position of the cathode tip and constrictor bore. This change in cathode configuration will affect the performance of arcjet thruster. In the experiments[4] the arc in the constrictor region of the nozzle was found to be off-centered due to which radial intensity profiles were not symmetric as shown in Figure 1. Although various experimental studies have been performed to study the influence of erosion[1,5,6] and off-centered cathode tip [4,6] on performance, but many physical quantities of interest cannot be probed using experimental techniques. This is where numerical models can help one obtain a clearer and more complete picture of various interacting physical phenomena.

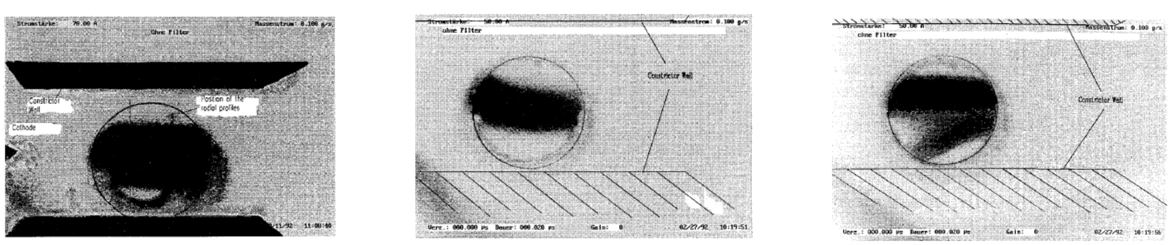

(a) symmetrically placed cathode (b) asymmetrically placed cathode (c) asymmetric constrictor bore

Figure 1. Illustration of arc inside the constrictor for asymmetric geometry [4]

Over the years various 2D/axisymmetric numerical models[7–10] of arcjet thruster have been developed by researchers. However, they are not capable of capturing the unsymmetrical plasma flow and heat transfer inside the thruster. Therefore, a 3D numerical model has been developed in this paper to study the effect of the off-centered cathode on the heat transfer and plasma flow.

II. Modeling Approach

The numerical model developed for simulating a 3D hydrogen arcjet thruster assumes that the thruster is operated in steady mode and that the gas flow in the arcjet thruster is laminar and compressible. Hydrogen plasma is optically thin, quasi-neutral ($n_i = n_e$) and in local thermal equilibrium. The convection velocity of all species in plasma is considered to be the same. The governing equations describing the essential physical processes in a hydrogen arcjet are describe next.

A. Governing Equations

The complete set of governing equations includes those of conservation of mass, momentum, and energy for a viscous, compressible flow with the electromagnetic body forces and Joule (Ohmic) heating as source terms in momentum and energy equations respectively. These equations in integral form over an arbitrary discrete control volume may be written as

Mass conservation equation

$$\frac{\partial}{\partial t}\oint \rho \, d\Omega + \oint \rho \boldsymbol{V}\cdot\boldsymbol{n} ds = 0 \tag{1}$$

Hydrogen ion conservation equation

$$\frac{\partial}{\partial t}\oint \rho y_{H^+} \, d\Omega + \oint \rho y_{H^+} \boldsymbol{V}\cdot\boldsymbol{n} ds = \oint m_{H^+}\dot{n}_{H^+} \, d\Omega + \oint D_{amb}\boldsymbol{\nabla}(\rho y_{H^+})\cdot\boldsymbol{n}\, ds \tag{2}$$

Hydrogen atom conservation equation

$$\frac{\partial}{\partial t}\oint \rho y_{H} \, d\Omega + \oint \rho y_{H} \boldsymbol{V}\cdot\boldsymbol{n} ds = \oint m_{H}\dot{n}_{H} \, d\Omega + \oint D_{H}\boldsymbol{\nabla}(\rho y_{H})\cdot\boldsymbol{n}\, ds \tag{3}$$

Momentum conservation equation

$$\frac{\partial}{\partial t}\oint \rho \boldsymbol{V} d\Omega + \oint \rho \boldsymbol{V}\cdot\boldsymbol{V}\cdot\boldsymbol{n} ds = -\oint P\,\boldsymbol{n} ds + \oint \bar{\bar{\boldsymbol{\tau}}}\cdot\boldsymbol{n} ds + \oint \mathbf{J}\times\mathbf{B}\, d\Omega \tag{4}$$

Energy conservation equation

$$\frac{\partial}{\partial t}\oint \rho e_{\boldsymbol{t}} d\Omega + \oint (\rho e_{\boldsymbol{t}} + P)\boldsymbol{V}\cdot\boldsymbol{n} ds = \oint (-\boldsymbol{q}\cdot\boldsymbol{n}) ds + \oint (\bar{\bar{\boldsymbol{\tau}}}\cdot\boldsymbol{V})\cdot\boldsymbol{n} ds + \oint \mathbf{J}\cdot\mathbf{E} d\Omega - \oint (L_h + L_e) d\Omega$$
$$\boldsymbol{q} = -\kappa_t \frac{dT}{dn} - \sum_i D_i h_i \frac{d\rho_i}{dn} \tag{5}$$

Equilibrium constants are given by Saha equation,

$$\frac{n_H^2}{n_{H_2}} = \frac{Z_{H,ex}^2}{Z_{H_2,ex}Z_{H_2,rot}Z_{H_2,vib}}\left(\frac{\pi m_H k_b T}{h^2}\right)^{1.5} exp\left(-\frac{\varepsilon_{d,H_2}}{k_b T}\right)$$
$$\frac{n_e n_{H^+}}{n_H} = 2\frac{Z_{H^+,ex}}{Z_{H,ex}}\left(\frac{\pi m_H k_b T}{h^2}\right)^{1.5} exp\left(-\frac{\varepsilon_{i,H}}{k_b T}\right) \tag{8}$$

The chemical process involves dissociation by joule heating of molecular hydrogen to atomic hydrogen and then ionization of atomic hydrogen to hydrogen ion.

Chemical reaction included in model and their kinetic parameter are mentioned in Table 1

Table 1 Chemical reactions and kinetic parameters

Reaction	Reaction rate coefficients	Loss rate (W/m3)	Ref
$2H + M = H_2 + M$	$k_{f1} = 1.764\times10^{-42}\times T^{-1}$	$L_h = \left(k_{b1}n_{H_2} - k_{f1}n_H^2\right)n_M\varepsilon_{d,H_2}$	[11]

$H^+ + e + M = H + M$	$k_{f2} = 1.45 \times 10^{-33} \times T^{-2.5}$	$L_h = \left(k_{b2} n_H - k_{f2} n_{H^+} n_e\right) n_M \varepsilon_{i,H}$	[11]
$H_2 + e \rightarrow 2H + e$	$k_{f3} =< \sigma v >$	$L_h = -1.34 k_{f3} n_e n_{H_2} \varepsilon_{d,H_2}$ $L_e = 2.34 k_{f3} n_e n_{H_2} \varepsilon_{d,H_2}$	[12]
$H^+ + e \rightarrow H + hv$	$k_{f4} = 6.26 \times 10^{-17} \times T^{-0.58}$	$L_e = k_{f4} n_{H^+} \varepsilon_{i,H}$	[11]
$H^+ + 2e = H + e$	$k_{f5} = 1.95 \times 10^{-20} \times T^{-4.5}$	$L_e = \left(k_{b4} n_H - k_{f5} n_{H^+} n_e\right) n_e \varepsilon_{i,H}$	[11]

Assuming induced magnetic field, Lorentz force and electron pressure gradient terms are negligible. Ohm's law and current conservation are used to solve for current density and electric potential.

$$\vec{J} = \sigma\left(-\vec{\nabla}\phi\right) \tag{9}$$

$$\vec{\nabla}.\vec{J} = 0 \Rightarrow \vec{\nabla}.\sigma\left(\vec{\nabla}\phi\right) = 0 \tag{10}$$

The governing equations are discretized using an unstructured cell-centered finite volume method. For the flow equations, 2nd order accurate AUSM+-up[13] scheme with Venkatakrishnan limiter[14] is used to compute convective fluxes. The gradient terms are calculated based on the least-square gradient method. After spatial discretization, the equations become ODEs in time. Then conservation equations are integrated using an explicit four-stage Runge-Kutta method.

3D steady-state Maxwell's equations combined with Ohm's law (neglecting Hall Effect and ion slip), Ampere's law (neglecting displacement current) gives the electric and magnetic potential equations. These governing equations are solved by the Finite Element Method (FEM) using the conjugate gradient method to determine the magnetic field and current density.

Thus, a two-way coupling is established between fluid solver and electromagnetic field solver. Ionization-recombination reaction in the plasma is considered only between neutral atom-electron collisions. Radiation heat transfer and electrical sheath formation at solid boundaries are neglected.

B. Transport coefficients

Transport coefficients are calculated using the mean free path mixture rules[15].The viscosity and thermal conductivity are computed as

$$\mu_t = \sum_{i=1}^{N}\left(\frac{n_i \mu_i}{\sum_{j=1}^{N} n_j \xi_{ij}}\right), \qquad \kappa_t = \sum_{i=1}^{N}\left(\frac{n_i \kappa_i}{\sum_{j=1}^{N} n_j \xi_{ij}}\right)$$
$$\xi_{ij} = \sqrt{\frac{2m_{ij}}{m_i}\frac{\overline{\Omega}_{ij}^{(2,2)}}{\overline{\Omega}_{ii}^{(2,2)}}} \tag{12}$$

pure species viscosity and thermal conductivity

$$\mu_i = 2.6693 \times 10^{-6}\frac{\sqrt{M_i T}}{\overline{\Omega}_{ii}^{(2,2)}}, \qquad \kappa_i = \frac{15}{4}\frac{\hat{R}}{M_i}\mu_i \tag{13}$$

The electron thermal conductivity is given by

$$\kappa_e = \frac{x_{H^+} \kappa_e \overline{\Omega}_{ee}^{(2,2)}}{x_{H^+} + \sqrt{2}\left(x_{H_2}\overline{\Omega}_{H_2 e}^{(2,2)} + x_H \overline{\Omega}_{He}^{(2,2)} + x_{H^+}\overline{\Omega}_{H^+ e}^{(2,2)}\right)} \tag{14}$$

and electrical conductivity is calculated from

$$\sigma = \frac{0.532\, n_e e^2}{\sqrt{m_e k_B T}\left(n_{H_2} Q_{eH_2} + n_H Q_{eH} + n_{H^+} Q_{eH^+} + n_e Q_{ee}\right)} \tag{15}$$

The diffusion coefficients D_i are mixture-averaged as

$$D_i = \frac{(1 - x_i)}{\sum_{j \neq i} x_j / D_{ij}} \tag{16}$$

$$D_{ij} = 2.628 \times 10^{-7} \sqrt{\frac{T^3(m_i + m_j)}{2m_i m_j}} \frac{1}{P\overline{\Omega}_{ij}^{(1,1)}}$$

The electron and ion diffusion coefficient are modified to the ambipolar diffusion coefficient

$$D_{amb} = \frac{D_{H^+}\mu_e n_e + \mu_{H^+} D_e n_e}{\mu_e n_e + \mu_{H^+} n_{H^+}} \tag{17}$$

Collision integrals and collision cross-section are obtained from Norman T G [16], Temperature-dependent curve fits are used for elastic collision data[17,18].

C. Boundary conditions

In this study, thruster geometry and mesh distribution as indicated in Figure 2. The boundary conditions for the continuity, momentum, energy, and electric potential equation are summarized in Table 2. For a subsonic inflow mass flow rate, inlet temperature is specified, and pressure is extrapolated from the computational domain. No-slip conditions are prescribed for velocity components, zero normal gradient of pressure is employed for electrode surfaces. The temperature along the anode surface is set to increase linearly from 1000 K from nozzle upstream to 1400 K at the nozzle exit[7,8]. At the anode surface, the diffusion velocities are equated to a fraction α_i $\left(\alpha_H = \alpha_{H^+} = 1,\ \alpha_{H_2} = 0\right)$ of the species thermal velocities[8]. Adiabatic wall condition is considered for the cathode. At the outflow boundary all the variables are extrapolated.

The anode is considered as the equipotential surface with voltage updated to maintain the current target. Whereas cathode modeled is equipotential surface. The voltage at outflow boundaries are gradients free.

Table 2 Boundary conditions at various boundary faces

Variable	Inlet	Outlet	Anode	Cathode
u	From stagnation properties	Extrapolated	0	0
v, w	0	Extrapolated	0	0
T	From $\dot{m}, T_{inlet}$	Extrapolated	Specified $T(x)$	$\frac{\partial T}{\partial n} = 0$
P	Extrapolated	Extrapolated	$\frac{\partial P}{\partial n} = 0$	$\frac{\partial P}{\partial n} = 0$
y_i	$y_{H_2} = 1, y_{i \neq H_2} = 0$	Extrapolated	$D_i \frac{\partial y_i}{\partial n} = \frac{\alpha_i}{4}\sqrt{\frac{8k_b T}{\pi m_i}}$	$\frac{\partial y_i}{\partial n} = 0$
ϕ	$\frac{\partial \phi}{\partial n} = 0$	$\frac{\partial \phi}{\partial n} = 0$	$\phi^{(n)}$	0

At each time step, the anodic electrical potential $^{(n)}$ is fitted to maintain the current target

$$I = \iint J \cdot ds\ , \qquad \phi^n = \frac{I_{target}}{I_{measured}} \phi^{n-1}$$

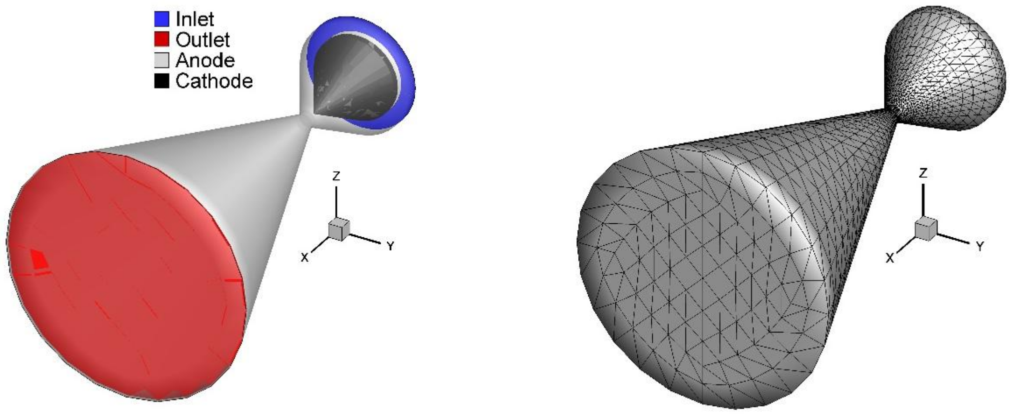

a) Geometry schematic b) grid

Figure 2. 3D Computational domain (a) Geometry schematic and (b) grid (0.5million)

III. Results and discussions

A. Model validation

In the process of CFD code development for arcjet, the code was also validated against standard compressible benchmarks like CD nozzle flow. The arcjet numerical model was validated by simulating an experimental study consisting of a 1 kW class arcjet thruster designed by NASA Glenn (formally Lewis) Research Center[19], The thruster has a 0.635 mm diameter, a 0.25mm long constrictor and a divergent conical nozzle with 20 half-angle and an area ratio of 225. A baseline case for simulation was thruster operating at hydrogen mass flow rate of 13 mg/s subjected to arc current of 10.3 A

The predicted results obtained by the model are presented in Figure 3. along with experimentally measured values from [19]. These results include radial profiles of the axial velocity, gas temperature and electron number density at the exit plane of arcjet. Figure 3(a) shows the predicted radial distribution of axial velocity at exit plane is compared with the experimental data of [19]. Similarly, a comparison of experimentally obtained data and numerically predicted data for the radial distribution of temperature[20] and number density of electron[20] at exit plane shown in Figure 3(b, c). It may be noted that the experimental results[19,20] were obtained at 0.4 mm downstream of the arcjet exit plane. One can note that there is a good agreement between computed and experimental results except some discrepancy in temperature which may be due to the assumption of local thermodynamic equilibrium.

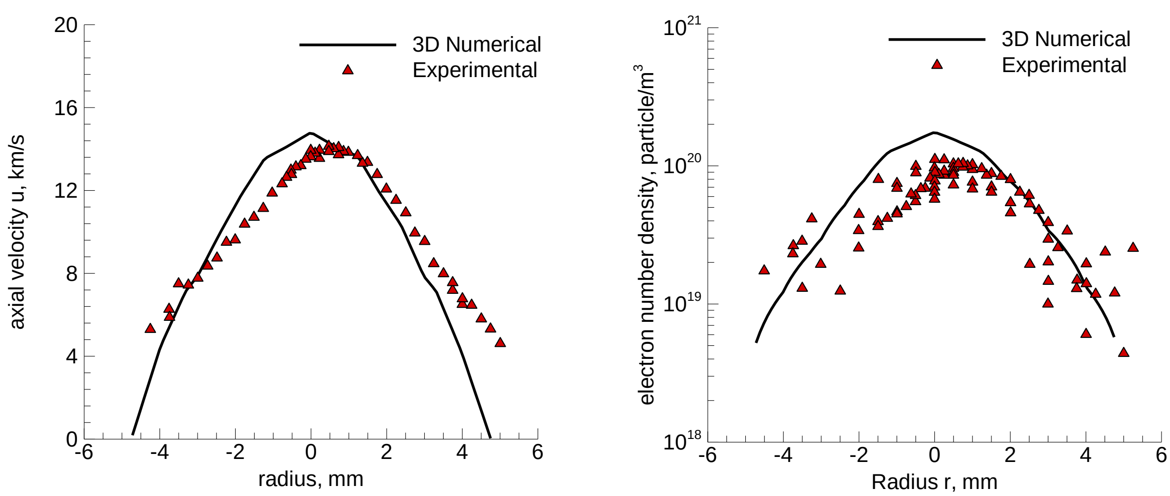

a) Axial velocity b) Electron number density

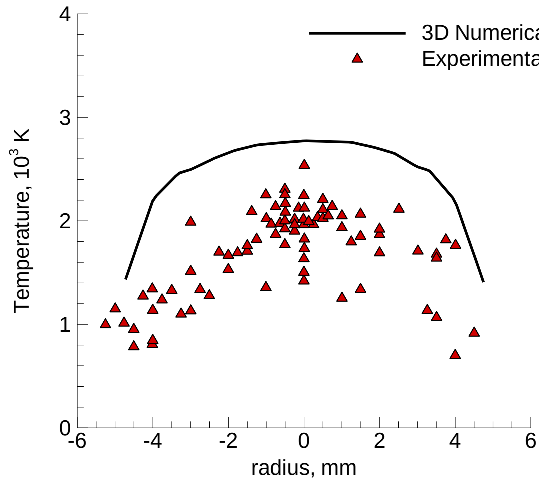

c) Temperature

Figure 3. Comparison of experimental and numerical data at the exit plane of arcjet thruster

B. Numerical study on the cathode: Effect of cathode tip offset from thruster axis

The performance of a thermal arc jet thruster is strongly determined by the processes near cathode tip and in the constrictor region. Glocker, [4] observed in their experiments with argon arcjet that an off-centered cathode resulted in unsymmetrical arc behavior in upstream but retained symmetry further downstream due to hydrodynamic pressure. Further in the experiments on hydrogen arcjet[1,21] it was noted that prolong use of arcjet thruster for few hundred hours resulted in cathode erosion which in turn resulted in change in the performance of the thruster. In this work objective is to provide a basic understanding of the arcjet performance when cathode is offset from the central axis.

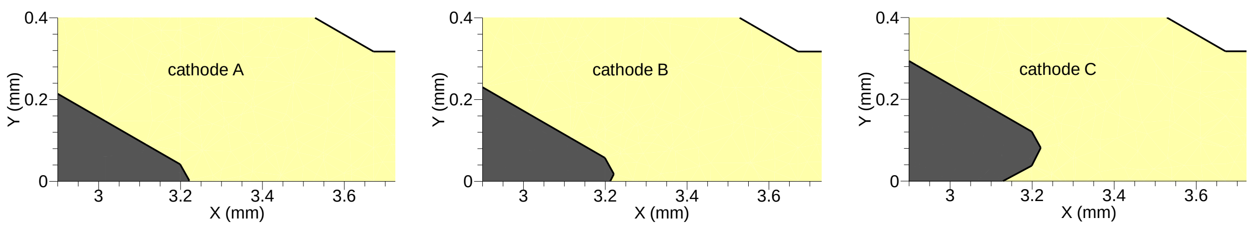

a) symmetric cathode b) 5% offset c) 25% offset

Figure 4. Cathode tip configurations (offset is % of constrictor radius by which tip is off axis)

In order to achieve the above stated objective a base geometry of NASA LeRC[19] hydrogen arcjet is considered. In this geometry for the base line case where cathode geometry symmetrically placed about the axis, is referred to as Cathode-A. Two other configurations are considered namely Cathode B, and cathode C, where cathode tip is unsymmetrically placed with cathode tips located at 5% and 25% of constrictor radius respectively from the axis of arcjet thruster. The three configurations are depicted in fig 4**Error! Reference source not found.** In all these 3 cases the other geometric and operating parameters remain the same. Hydrogen inlet mass flow rate is of 13 mg/s and arc current of 10.3 A

In a typical arcjet operation, the potential difference between electrodes forms the electric field which accelerates the electron inside thruster from higher potential to lower potential. With the help of the collisions, the electrons transfer the energy to heavy species. The electric field is very high at the cathode tip, causing the electrons to accelerate more near the cathode tip. This gives rise to high current density and joule heating near the cathode tip. After absorbing energy by joule heating, the flow accelerates in downstream of the nozzle. Figure 5 shows contours of current density, and joule heating per unit volume of plasma/gas on a plane (referred here a 'Z' plane) containing axis of thruster and the axis of cathode (which may be offset from the axis of the thruster). Also shown are current densities at various planes perpendicular to the thruster axis (X planes). One can note high current densities and thus Joule heating per unit volume at the cathode tip. While the contours are symmetrical for Cathode-A, a slight asymmetry in contours can be noted in case of Cathode-B case and visibly distinct asymmetry in contours of cathode-C configuration. The arc is seen to bend toward the anode wall closer the offset cathode. It is also noted that as the gas/plasma moves downstream the asymmetry is seen to reduce possibly due to high dynamic pressure of plasma in downstream the joule heating region. The contours of temperature (see Figure 6) and contours of velocity (see Figure 7) are seen to follow the same trend. However, some asymmetry in temperature and velocity even at the exit plane.

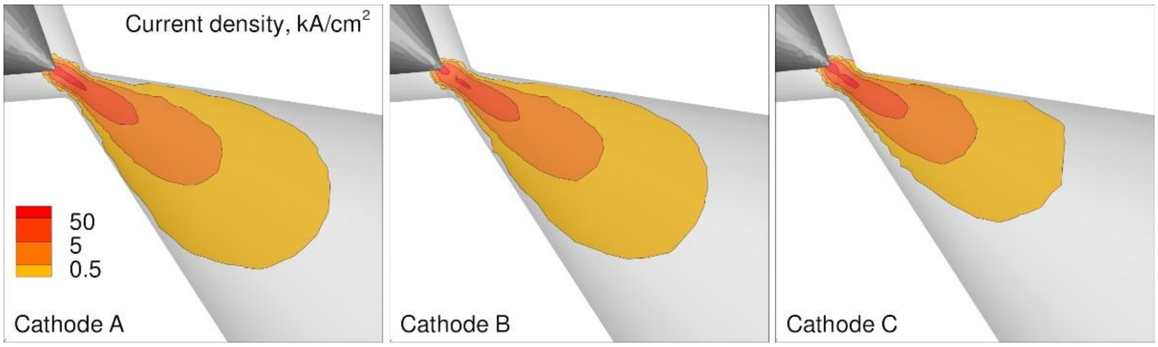

a) current density along Z-plane

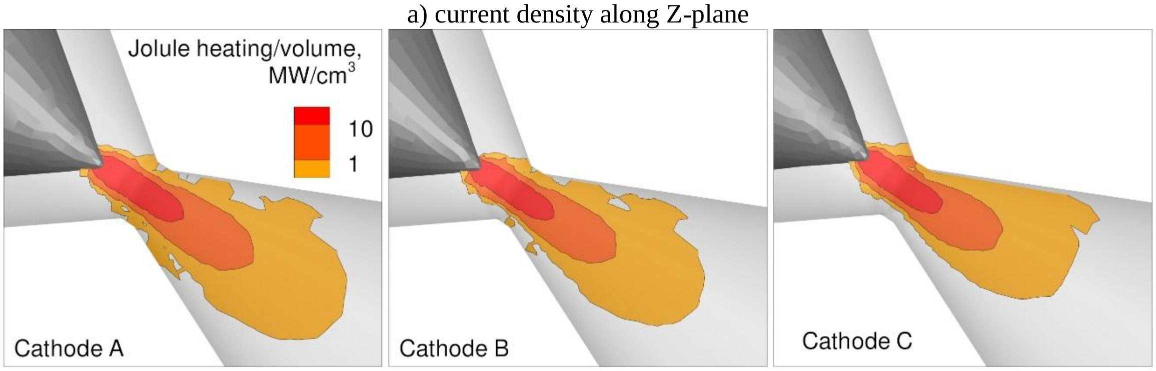

b) Joule heaing/volume along Z-plane

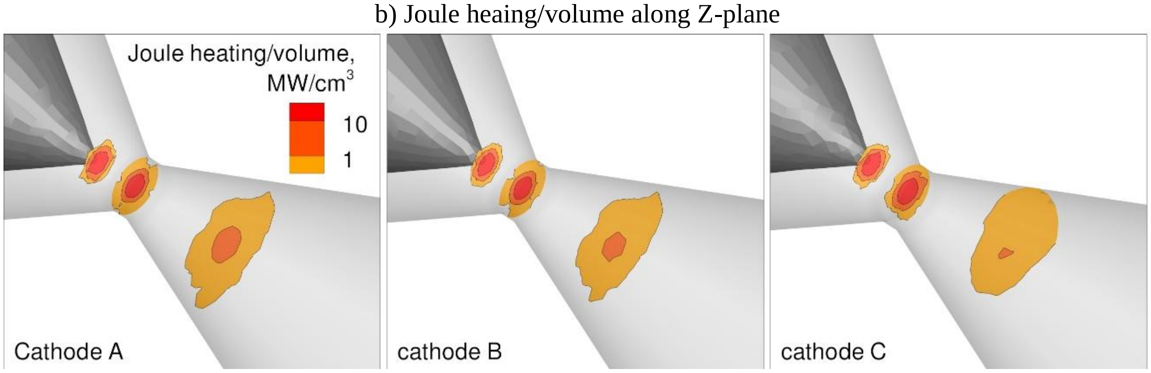

c) Joule heaing/volume along X-planes

Figure 5. Computed current densities and Joule heating/volume for cathode A, cathode B, and cathode C configurations.

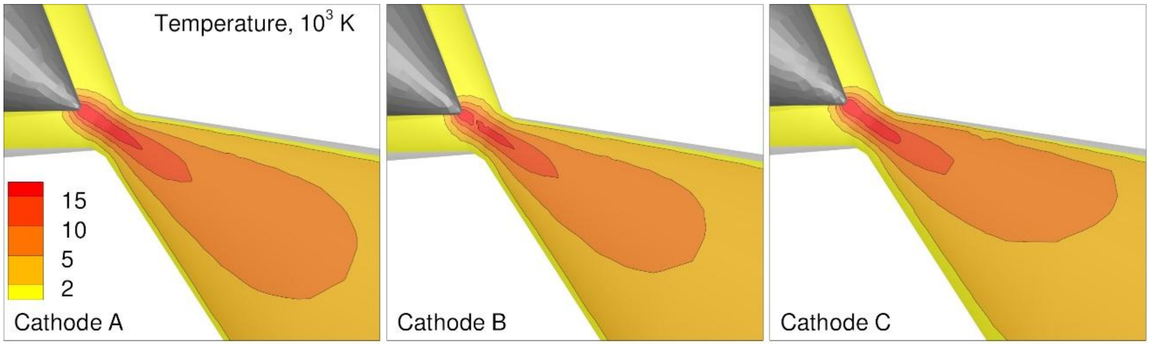

a) Temperature along Z-plane

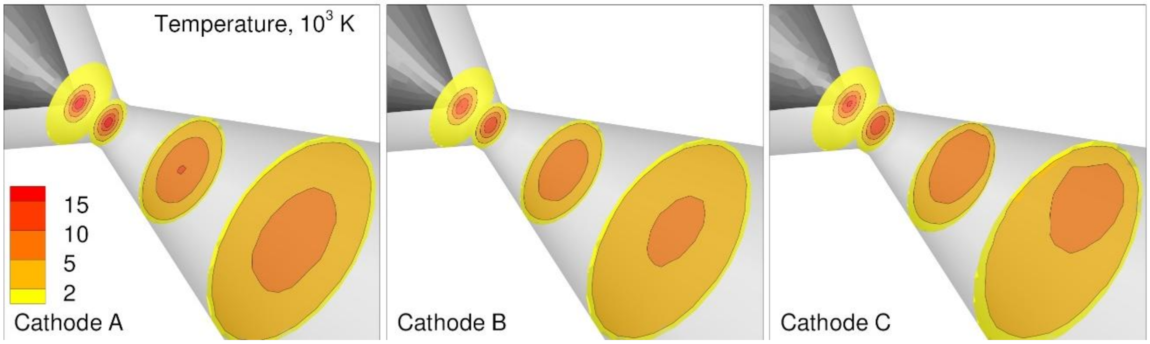

b) Temperature along X-planes

Figure 6. Computed temperature for cathode A, cathode B and cathode C, configurations.

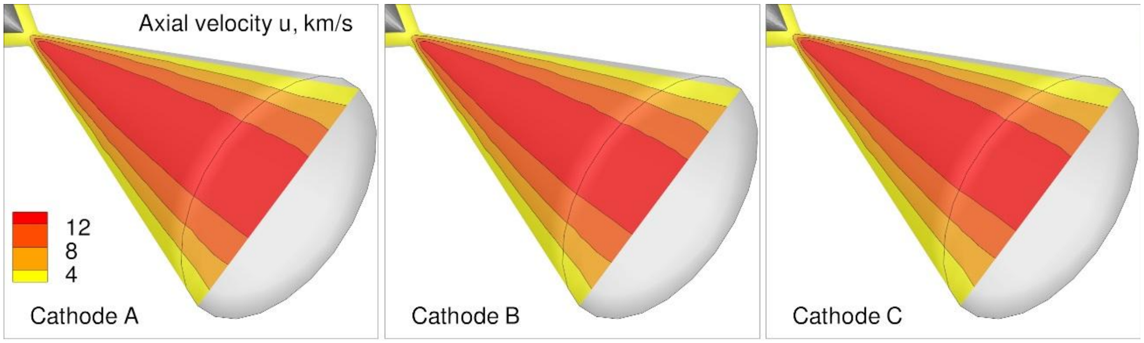

a) Axial velocity along Z-plane

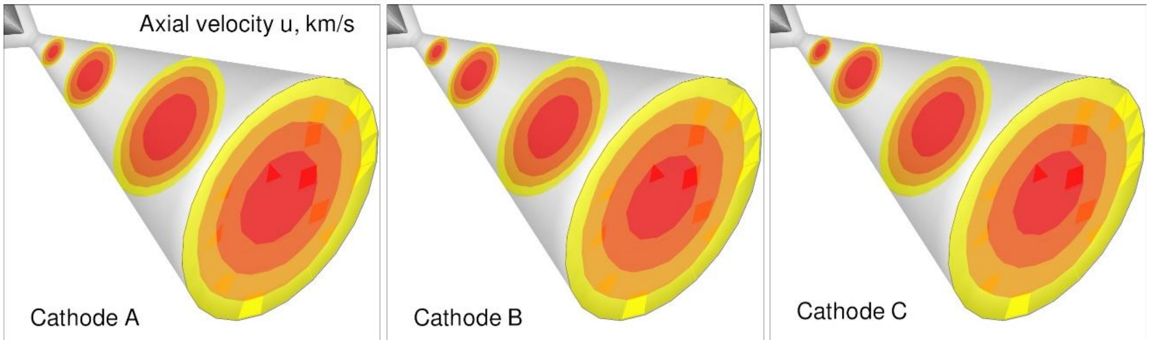

b) Axial velocityalong X-planes

Figure 7. Computed axial velocity for cathode A, cathode B and cathode C, configurations

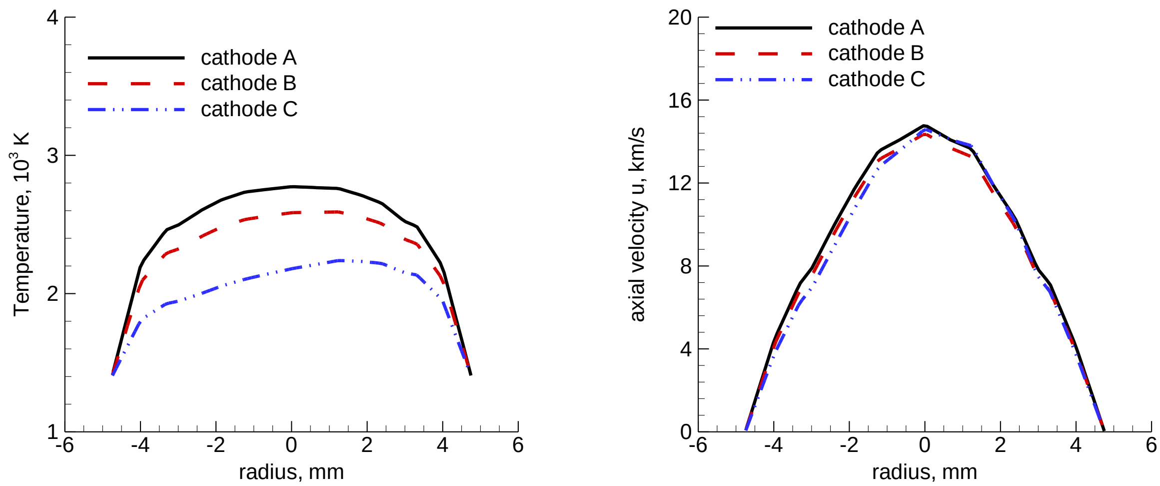

a) Temperature b) Axial velocity

Figure 8 Comparison of (a) temperature and (b) axial velocity at nozzle exit plane for cathode-A, cathode-B and cathode-C configurations

Since there is asymmetry in the temperature and the axial velocity (although much less compared to temperature) distribution at the exit plane, one can expect change in thruster performance and also presence of side thrust normal to axis in the direction of cathode offset. Therefore, it is useful to evaluate change in the performance of the thruster for the three cases. Table 3 present total thrust and specific impulse (I_{sp}) for the three cases. Also included is the side thrust or thrust normal to the axis of thruster due to cathode offset

Table 3 Thruster specific impulse for various cathode confihgurations

Configuration	Thrust in X (mN)	Thrust in Y (mN)	Pressure thrust(mN)	Total thrust	I_{sp} (s)	Percentage change in I_{sp}
Cathode A	129.2	0	20.46	149.4	1108	-
Cathode B	119.6	0.35	18.72	138.3	1077	-2.8
Cathode C	119.2	2.98	16.7	137.3	1070	-3.4

It is interesting to note that even for large offset as 25% (cathode-B) there is no significant loss of thrust loss of thrust or specific impulse. However, a small normal thrust will exist when there is cathode offset away from the axis of the thruster. The side thrust obtained case of cathode-B (5 % offset) and in case of cathode-C (25% offset) was 0.35 mN and 2.98 mN respectively.

IV. Conclusion

In the present work a model for hydrogen arcjet assuming local thermal equilibrium was formulated and a 3D numerical CFD code was developed and validate against existing experimental data to assess the effect of cathode configuration (here cathode tip offset from the thruster axis) on thruster performance. The following conclusion may be derived from this study.

1. For the case of perfectly aligned cathode, where the cathode axis aligns with thruster axis and cathode tip is on the thruster axis, the computed current density and Joule heating in the thruster shows a symmetric distribution about the axis of the thruster and so are the temperature and velocity profiles.

2. When the cathode tip is offset from the axis of the thruster, an asymmetry develops in current distribution between cathode and anode and consequently in temperature and velocity profiles. However, downstream of the constrictor where the flow accelerates the asymmetry decays owing to high dynamic pressure. However, if the offset I large (as in case of 25 % offset case of cathode-C), the asymmetry in temperature

and velocity field may be carried over to the exit plane. This also results inside force on the thruster in the direction of the offset. However, the magnitude of the side was found to be small (about 2.5 mN for the case of cathode-C).

3. It was noted from this study that thruster performance (thrust and I_{sp}) decreases only marginally due to cathode offset.

Acknowledgments

The authors acknowledge support of Indian Space Research Organization for this study under technical monitoring of Shri L Aravaindakshan Pillai and Shri Pedda Peeraiah C.

References

[1] Curran FM, Haag TW. Extended life and performance test of a low-power arcjet. Journal of Spacecraft and Rockets 2008;29:444–52. doi:10.2514/3.25484.
[2] Koroteev AS, Blagov V V., Lomovtsev MA. ARC JET THRUSTERS. Acta Astronautica, 1993, p. 37–9.
[3] Sankovic J, Jacobson D. Performance of a miniaturized arcjet. 31st Joint Propulsion Conference and Exhibit, Reston, Virigina: American Institute of Aeronautics and Astronautics; 1995. doi:10.2514/6.1995-2822.
[4] Riehle M, Glocker B, Auweter M, Kurtz H. Development of a Thermal Arcjet. Cleveland, Ohio: 1993.
[5] Gilz TM, Auweter-Kurtz M, Kurtz HL, Schrade HO. High Power Arcjet Thruster Experiments n.d.
[6] Haag TW, Curran FM. Arcjet Starting Reliability: A Multistart Test on Hydrogen/Nitrogen Mixtures.IEPC 87-1061
[7] Sun W-P, Wei F-Z, Wang H-X. Numerical Simulation of Nonequilibrium Flow in a Low-Power Hydrogen Arcjet. 33rd International Electric Propulsion Conference, 2013, p. 406.
[8] Megli TW. A nonequilibrium plasmadynamics model for nitrogen/hydrogen arcjets. University of Illinois at Urbana-Champaign, 1995.
[9] Hardy TL, Curran FM. Low Power dc Arcjet Operation With Hydrogen / Nitrogen / Ammonia Mixtures 2019.
[10] Hari Prasad N, Amit K, Jayachandran T, Peeraiah P. Numerical Modeling of Arcjet Thruster : Effect of Design & Operating Parameters on Arc Heating. International Electric Propulsion Conference, Georgia: 2017, p. 532.
[11] Mccay TD, Dextert CE. Chemical Kinetic Performance Losses for a Hydrogen Laser Thermal Thruster. Journal of Spacecraft and Rockets n.d.;24:372–6.
[12] Janev RK, Langer WD, Evans k., Post D.E. Elementary processes in hydrogen-helium plasmas: cross sections and reaction rate coefficients. vol. 4. 2012.
[13] Liou MS. A sequel to AUSM, Part II: AUSM+-up for all speeds. Journal of Computational Physics 2006;214:137–70. doi:10.1016/j.jcp.2005.09.020.
[14] Blazek J. Computational fluid dynamics:Principles of Grid Generation. First edit. Elsevier Ltd; 2001.
[15] Kruger M and. Partially Ionized Gases. John Wiley & Sons. New York; 1973.
[16] Norman T G. Calculation of transport properties of ionizing atomic hydrogen. Nasa Technical Note 1966.
[17] Macdonald J. Accurate collision integrals for the attractive static screened coulomb potential with application to electrical conductivity. vol. 76. 1991.
[18] Paquette C, Pelletier C, Fontaine G, Michaud G. Diffusion coefficients for stellar plasmas. vol. 17. 1986.
[19] Liebeskind JG, Hanson RK, Cappelli M a. Laser-induced fluorescence diagnostic for temperature and velocity measurements in a hydrogen arcjet plume. Applied Optics 1993;32:6117. doi:10.1364/AO.32.006117.
[20] Storm PV, Cappelli MA. Stark broadening corrections to laser-induced fluorescence temperature measurements in a hydrogen arcjet plume. Applied Optics 1996;35.
[21] Haag TW, Curran FM, Haag TW, Curran FM. High-Power Hydrogen Arcjet Performance 2019.